Effect of higher modes and multi-directional seismic excitations on power plant liquid storage pools

M. Eswaran[*], G.R. Reddy and R.K. Singh

*Structural and Seismic Engineering Section, Reactor safety Division,
Bhabha Atomic Research Centre, Mumbai, 400085, India*

Abstract. The slosh height and the possibility of water spill from rectangular Spent Fuel Storage Bays (SFSB) and Tray Loading Bays (TLB) of Nuclear power plant (NPP) are studied during 0.2 g, Safe Shutdown Earthquake (SSE) level of earthquake. The slosh height obtained through Computational Fluid dynamics (CFD) is compared the values given by TID-7024 (Housner 1963) and American concrete institute (ACI) seismic codes. An equivalent amplitude method is used to compute the slosh height through CFD. Numerically computed slosh height for first mode of vibration is found to be in agreement the codal values. The combined effect in longitudinal and lateral directions are studied separately, and found that the slosh height is increased by 24.3% and 38.9% along length and width directions respectively. There is no liquid spillage under SSE level of earthquake data in SFSB and TLB at convective level and at free surface acceleration data. Since seismic design codes do not have guidelines for combined excitations and effect of higher modes for irregular geometries, this CFD procedure can be opted for any geometries to study effect of higher modes and combined three directional excitations.

Keywords: liquid sloshing; SSE level earthquake; free surface; CFD; higher modes

1. Introduction

Nuclear power plants and many oil and gas industries make use of liquid storage tanks for storing liquids like water, oil, chemical fluids and wastes of different forms. These tanks are exposed to a wide range of seismic hazards and interaction with other sectors of built environment. Heavy damages have been reported due to strong earthquakes as evident in Niigata in 1964, Alaska in 1964, Parkfield in 1966, Imperial County in 1979, Coalinga in 1983, Northridge in 1994, and Kocaeli in 1999 (Towhata 2008, Vosoughifar and Naderi 2014). Rectangular and circular tanks are very popular for storing liquid and etc. Liquid oscillations will occur inside the pool, at the time of earthquake. These free surface oscillations of liquid inside the pool are termed sloshing. When the fluid oscillation frequency coincides with the first mode natural frequency of the tank, resonance will occur. Then, large liquid sloshing will take place.

As reported by Shimada *et al*. (1988), large sloshing heights are recorded during 1983 Nihonkai-chubu earthquake. It was found that the estimated sloshing heights under nonlinear

---

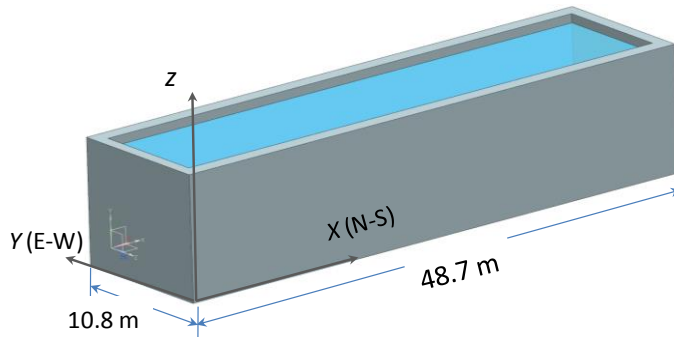[*]Corresponding author, Scientific Officer, E-mail: eswaran@barc.gov.in
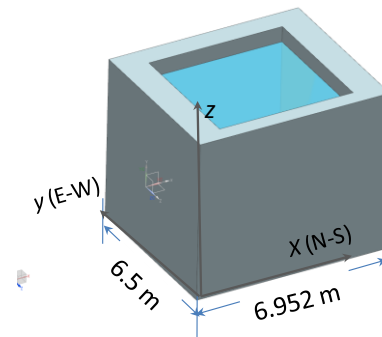
Fig. 1 Spent fuel storage bays

Fig. 2 Tray loading bay

conditions are around 10-40% larger than those calculated under linear conditions. In current seismic design codes, the vertical excitation are usually taken as two thirds of the horizontal response spectra. But the recent studies have shown that vertical to horizontal response spectral ratio depends on the source to site distance. The ratio is higher in the near-field region as well as in the high frequency range of the response spectra (Kianoush and Chen 2006).

Seismic design codes do not have guidelines for the effect of higher modes and combined excitations on the slosh height. Hence, the effect of higher modes and combined excitations are studied through CFD using nonlinear Navier Stokes equation. Optimum tank design and random excitation investigations are still ongoing topics due to its practical importance and to address the safety issues. Recently, Yousefi *et al*. (2014) and Xu *et al*. (2011) are simulated for optimal design of fuel tank and fully nonlinear sloshing waves in three-dimensional tank under random excitation respectively.

A typical nuclear power plant has Spent Fuel Storage Bays (SFSB) and Tray Loading Bays (TLB). SFSB is located inside the fuel building (i.e., outside Reactor Building). Usually, it has the capacity to store spent fuel bundles of 10 years reactor operation and one emergency full core unload. Here, for this liquid sloshing study, a typical reactor SFSB and TLB dimensions have been taken. SFSB pool dimensions are 48.445 m×10.8 m×9.5 m and still water level is 8.7 m as shown in Fig. 1. Water inventory inside the SFSB is about 4500 m^3. Free board height of SFSB is 0.8 m. Similarly, TLB dimensions are 6.9 m×6.5 m×6.5 m and still water level is 5.7 m as shown in Fig. 2. Free board is 0.8 m. The slosh height under design earthquake called SSE and the possibility of spillover of water from SFSB and TLB during SSE level of earthquake needs to be evaluated.

The present work is focused on a long rectangular tank (SFSB) and a cubic tank (TLB). The natural frequencies of fluid in the SFSB pool and TLB are evaluated using TID-7024, ACI 350.3 (2001) codes and CFD approach. The effect of higher modes and combined excitations on slosh height under first mode and higher modes are estimated using CFD. The slosh height is determined for SSE inputs at convective level and at free surface level. The effect of vertical excitation and also a combined (Two horizontal and one vertical) excitation in the pools are studied in detail. The time-frequency information has been observed by using wavelet analysis. In the field of fluid dynamics the use of wavelet analysis is used to identify the frequencies. Alam and Sakamoto (2003) used wavelet to show how the wake frequency of a cylinder changes with respect to that of another with respect to time and for different staggered arrangements of cylinders.

Slosh height is usually computed for the Floor response spectrum (FRS) data of corresponding pool for seismic design of liquid tank. FRS data for SFSB at convective height and at free surface
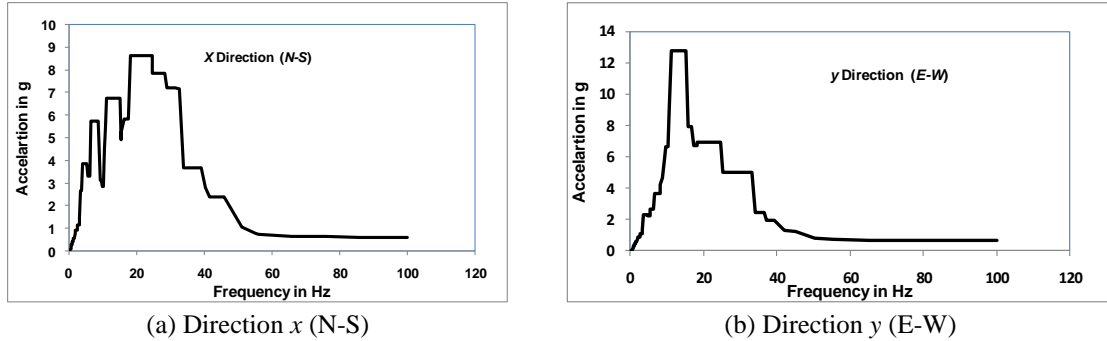
(a) Direction x (N-S)

(b) Direction y (E-W)

Fig. 3 SSE level FRS at convective height for 0.5% damping for SFSB

(a) Direction x (N-S)
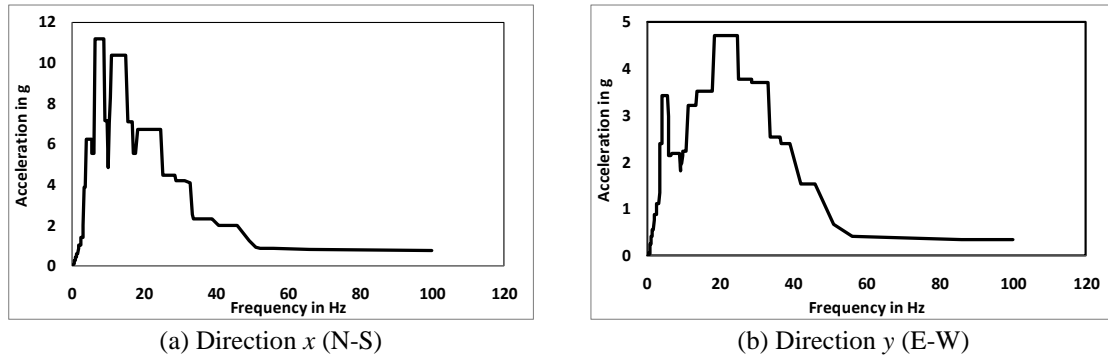
(b) Direction y (E-W)

Fig. 4 SSE level FRS at liquid free surface level for 0.5% damping for SFSB

(i.e., tank top level) is shown in Fig. 3(a) and (b) and Fig. 4(a) and (b) respectively. This FRS data is generated for a plant SFSB site.

2. Methodology

2.1 Computation of slosh height using CFD

Slosh height is computed from the numerical solutions of the unsteady Navier-Stokes equations. The continuity and momentum equations are solved using finite volume method. The free surface is captured by Volume of Fluid (VOF) technique. The model on the fluid domain is based on the three-dimensional time-dependent conservation equations of mass and momentum to determine the sloshing characteristics. The forces acting on the fluid in order to conserve momentum must balance the rate of change of momentum of fluid per unit volume. For the transient laminar, incompressible flow with constant fluid properties over the computational domain, the mass continuity and Navier–Stokes equations are given as follows.

$$\nabla \cdot \vec{u} = 0 \tag{1}$$

$$\rho \left(\frac{\partial \vec{u}}{\partial t} + \vec{u} \cdot \nabla \vec{u} \right) = -\nabla P + \mu \nabla^2 \vec{u} + \vec{F} \tag{2}$$

where $\vec{F}$ is the external force vector and μ, ρ are the dynamic viscosity and density of the fluid respectively. The external force is the sum of the gravitational and applied forces. The $\vec{u}$ and P denote the velocity vector and pressure of the oscillating fluid. The aforementioned governing equations are discretized by the finite control volume approach to replace the partial differential equations with the resulting algebraic equations for the entire calculation region. Using the staggered-grid arrangement, grids of velocities are segregated from grids of scalars and laid directly on the surfaces of the control volumes for estimating those convective fluxes across cell surfaces. The well-known Semi-Implicit Method for Pressure-Linked Equations Consistent (SIMPLEC) numerical algorithm is employed for the velocity–pressure coupling. In SIMPLEC, an equation for pressure-correction is derived from the continuity equation which governs mass conservation. It is an inherently iterative method. The under-relaxation technique is also implemented to circumvent divergence during iterations. The velocities and local pressure can be determined until convergent criteria are satisfied.

For modelling free surface flows, marker and cell (Chen *et al*. 1997), VOF, level set method, sigma-transformation (Frandsen 2004, Eswaran and Saha 2009, 2010, 2011) and meshless method based on smoothed particle hydrodynamics (Vorobyev *et al*. 2011) are well-known methods. Nevertheless, this work adopts VOF method with Compressive Interface Capturing Scheme for Arbitrary Meshes (CICSAM). The original VOF method was developed by Hirt and Nichols (1981) and refined thereafter by various authors. Since the method is designed for two or more immiscible fluids, a portion of air is filled above the liquid level for all cases. The air portion is also modeled and discretized using the 3-D fluid element. In this method, the term, first fluid and second fluid indicate the air and water domains respectively. It is based on tracking a scalar field variable *f* which stands for the distribution of the second fluid in the computational grid. *f* specifies the fraction of the volume of each computational cell in the grid occupied by the second fluid. All cells containing only fluid 2 will take the value *f*=1 and cells completely filled with fluid 1 will be represented by *f*=0. Cells containing an interface between air and water take on a value of *f* between 0 and 1. For a given flow field with the velocity vector $\vec{u}$ and an initial distribution of *f* on a grid, the volume fraction distribution *f* (and hence the distribution of fluid two) is determined by the passive transport equation

$$\frac{\partial f}{\partial t} + \nabla \cdot (\vec{u}f) = 0 \tag{3}$$

This equation must be solved jointly with the primary equations (Eqs. (1), (2)) of conservation of mass and momentum, to achieve computational coupling between the velocity field solution and the liquid distribution. From the *f* distribution the interface between the two fluid phases has to be reconstructed at every time step. The simulation was carried out on an Intel Xeon, 2.8 GHz twenty core processor workstation and the simulation time was approximately 32 CPU hours for each case (solution up to 20 seconds). The implicit scheme is used for temporal integration and the higher order upwind schemes are used for the spatial discretization. The free surface elevation (ζ) has been captured every 0.05 second.

2.2 Computation of slosh height using international seismic design codes

The relations for assessing the maximum sloshing wave height are taken from TID 7024 and ACI. Free board height in a tank must be chosen based on the maximum value of sloshing wave height. This is particularly important for tanks containing radioactive liquids, where loss of liquid

are permitted by any means. If sufficient free board is not provided, the roof structure should be designed in such a manner to resist the uplift pressure due to sloshing of liquid. Moreover, if there is obstruction to free movement of convective mass due to insufficient free board, the amount of liquid in convective mode will also get influenced. More information regarding loads on roof structure and modified convective mass can be obtained in Malhotra (2004). However, the pools considered in this work, do not have roof.

For the purposes of incorporating the dynamic effects of sloshing in the pools, it is convenient to replace the liquid conceptually by an equivalent linear mechanical system. The equations of motion of oscillating masses and rigid masses are included more easily in the analysis than are the equations of fluid dynamics. Fig. 5 illustrates generalized spring-masses model for the rectangular tank and the symbols used in the analysis. The width of the tank are $2L$ and height of the liquid is denoted as h. The center of the mass of the liquid is represented as C.G, while, the locations (H_n) of the masses are references to the C.G. The tank is excited by a small time-varying linear acceleration $\ddot{X}_g$. Rigidly attached mass is denoted as m_0, while the convective (slosh) masses are showed as m_1 through m_n .The deflection of the mass is represented as x_n which is relative to the tank walls as a result of the tank motion.

2.3 Mathematical formulations for spring- mass model

The mathematical equations can be derived from static and dynamic properties of Spring- mass model. These equations and derivations can be found in ACI, Housner (1963) and Dodge (2000) for simple geometries like rectangular and cylindrical tanks. According to static properties, the sum of all the masses must be equal to the liquid mass and center of mass of the model must be same elevation as the liquid. These can be derived as follows

$$m_0+m_1+m_2+\dots+m_n=m_{liq} \tag{4}$$

$$m_0H_0+m_1H_1+m_2H_2+\dots+m_nH_n=0 \quad \text{at C.G} \tag{5}$$
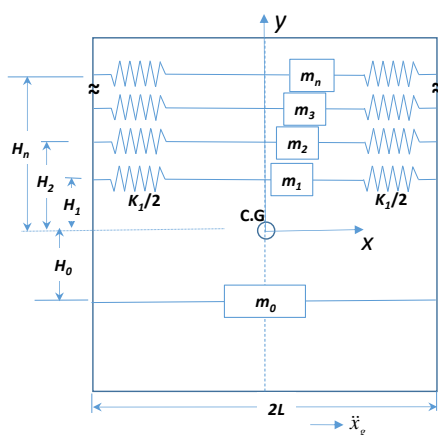

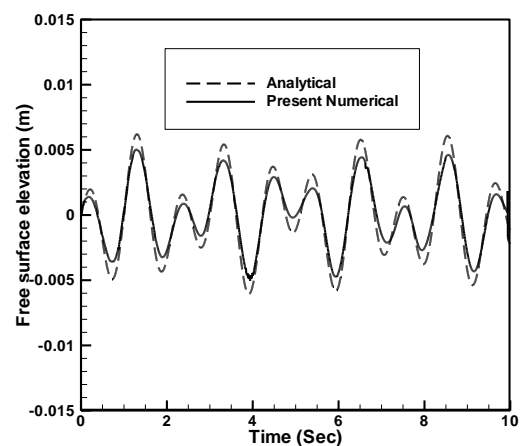Fig. 5 Schematic of equivalent spring-masses model for a rectangular tank

Fig. 6 Comparisons of free surface elevation

Equation of motion can be derived by inserting the acceleration terms and applying static properties into the force equation. The equations of motion for each of the spring-masses is expressed as

$$m_n\left(\ddot{X}_g + \ddot{x}_n\right) + k_n x_n = 0 \qquad (6)$$

From the above equations forces acting on the rectangular tank can be estimated. The slosh height is estimated using the well derived equations as listed here (Eqs. (7) to (13)). The Convective and impulsive masses are

$$m_n = m_{liq}\frac{8L\tanh(2n-1)\pi h/L}{\pi^3(2n-1)^3 h}. \qquad (7)$$

$$m_0 = m_{liq}\left[1 - \frac{8L\tanh(2n-1)\pi h/L}{\pi^3(2n-1)^3 h}\right]. \qquad (8)$$

Height of the convective masses and natural frequency

$$H_n = \frac{h}{2} - \frac{L}{(2n-1)\pi}\left[\tanh(2n-1)\pi h/2L - \frac{1}{\sinh\dfrac{(2n-1)\pi h}{L}}\right]\frac{8L\tanh(2n-1)\pi h/L}{\pi^3(2n-1)^3 h}. \qquad (9)$$

$$\omega = \sqrt{\frac{1.58g}{L}\tanh\left(1.58\frac{H}{L}\right)} \qquad (10)$$

The first mode slosh height

$$d_{n=1,max} = \frac{0.527L\coth(1.58 h/L)}{\dfrac{g}{\omega^2\theta_h L}-1} \quad \text{where, } n=1 \qquad (11)$$

and higher mode slosh height is

$$d_{n\,max} = 1.58 A_n \tanh(1.58 h/L), \quad \text{where, } n = 2, 3 \dots, \qquad (12)$$

here

$$A_n = S_n/\omega_n \qquad (13)$$

where S is the spectral acceleration co-efficient and ω_n is the slosh natural frequency of the nth mode. The maximum slosh height for n^{th} mode is $d_{n\,max}$. A_n is the maximum displacement of the nth convective mass.

2.4 Introduction to wavelet analysis

The Fourier transforms provide the spectral coefficients which are independent of time i.e., they can give the amplitude-frequency information and does not have any information about frequency with respect to time. Thus, it is useful only for a stationary signal where the amplitude-

frequency does not change with time. But, in real life cases the signals are time dependent and also non-stationary. In such cases, a scan analysis using the Short Term Fourier Transform (STFT) will be taken. But STFT has its limitations like it can give information only about the amplitude and frequency, but not anything about the time and frequency relation. However, wavelet transform gives a better idea about the time-frequency information about the signals. The wavelet transform is a linear convolution of a given one dimensional signal which is to be analysed and the mother wavelet $\psi(t)$. Mathematically a wavelet transform is as shown below (Fugal 2009).

$$W(s,b) = \frac{1}{\sqrt{s}} \int p(t)\psi^* \left(\frac{t-b}{s} \right) dt \qquad (14)$$

Where, $W(s,b)$ is the wavelet coefficient, the asterisk sign denotes the complex conjugate, 'b' is the translation parameter and 's' is the scale parameter. Generally, Gabor wavelet, Mexican hat wavelet, and Morlet wavelet are used in the field of fluid dynamics as a mother wavelet. In this study the Morlet wavelet has been used which is given by

$$\psi(\mathbf{t}) = \pi^{-\frac{1}{4}} \mathbf{e}^{i\omega_o \mathbf{t}} \mathbf{e}^{-(\omega_o \mathbf{t}/\gamma)^2/2} \qquad (15)$$

where $\gamma = \sqrt{2/ln(2)}$ and ω_o is the number of wave in the wavelets. In practise the value of ω_o varies from 5 to 12 and generally it is taken as 6. A frequency resolution of 12 is chosen when frequency of resolution of a signal is more important than time resolution. Recently, Bedaoui *et al.* (2014) is used wavelet tools for the frequency domains for dynamic signals.

3. Results and discussion

3.1 Validation studies

Initially to validate the procedure followed in this work as discussed in section 2.1, a 2-D partially filled tank has been taken and the liquid elevation has been captured under sinusoidal excitation by numerical as well as analytical relation. The 2-D rigid tank which is 570 mm long and 290 mm high is excited with $A\sin(\omega t)$. The water depth is 150 mm and excited amplitude is 5 mm. The lowest natural frequency ω_1 for this case is around 6 rad/sec. The natural frequency is calculated from Eq. (17). Liquid free surface elevation has been calculated from the following third order analytical relations (Eq. 16) (Faltinsen *et al.* 2000), and compared with the present numerical simulation results for frequency ratio 0.58.

$$\zeta(x,t) = a \left(\cos(\omega_n t)\cos(k_n x) + \frac{a\omega_n^2}{g} \left(\begin{array}{c} \left(\frac{1}{8} \frac{\omega_n^4 + g^2 k_n^2}{\omega_n^4} + \left(\frac{1}{8} \frac{3\omega_n^4 - g^2 k_n^2}{\omega_n^4} - \frac{3}{2} \frac{\omega_n^4 - g^2 k_n^2}{\omega_n^2(4\omega_n^2 - \omega_{2n}^2)} \right) \right) \\ * \cos(2\omega_n t) + \frac{1}{2} \frac{\omega_n^2 \omega_{2n}^2 - \omega_n^4 - 3g^2 k_n^2}{\omega_n^2(4\omega_n^2 - \omega_{2n}^2)} \cos(\omega_{2n} t) \end{array} \right) \cos(2k_n x) \right) \qquad (16)$$

where the linear sloshing frequencies,

$$\omega_n = \sqrt{gk_n \tanh(k_n h_s)} \quad \text{and} \quad \omega_{2n} = \sqrt{g2k_n \tanh(2k_n h_s)} \,. \qquad (17)$$

From Fig. 6, it is observed that the free surface elevation of analytical and present numerical

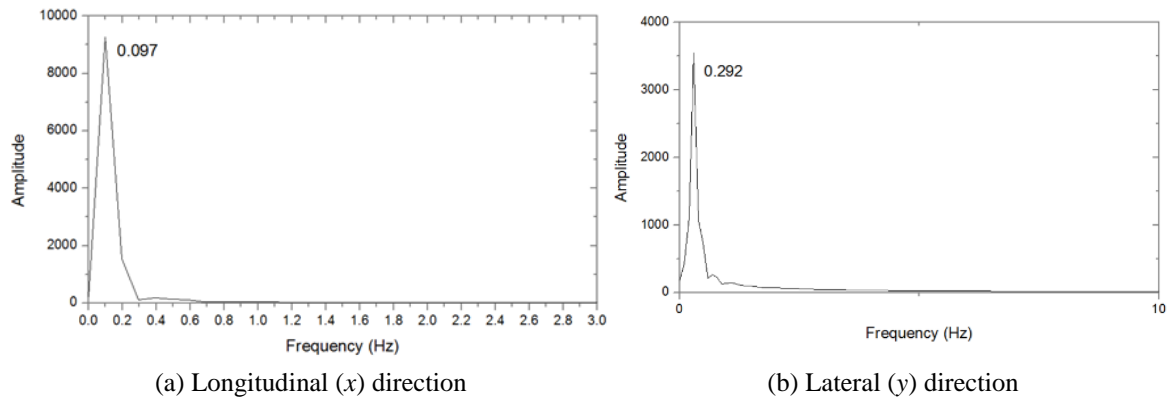(a) Longitudinal (*x*) direction   (b) Lateral (*y*) direction

Fig. 7 SFSB first mode frequencies obtained from free vibration data

Table 1 Sloshing frequencies for SFSB and TLB using CFD and analytical.

Mode	Frequency in Hz							
	SFSB				TLB			
	Length direction (*x*)		Width direction (*y*)		Length direction (*x*)		Width direction (*y*)	
	CFD	Analytical*	CFD	Analytical*	CFD	Analytical*	CFD	Analytical*
1	0.097	0.0912	0.292	0.2681	0.332	0.3337	0.345	0.341
2	0.213	0.212	0.464	0.462	0.473	0.477	0.490	0.488
3	0.283	0.272	0.600	0.5935	0.579	0.576	0.600	0.589
4	0.34	0.3358	0.722	0.7098	0.669	0.658	0.693	0.678

*Analytical values are computed from Eq. (17)

coincides with each other. Analytical equations are based on linear formulations. Since non-linearity exist in the CFD equations, a very small discrepancy near trough and crest of the free surface wave in Fig. 6.

3.2 Computation of modal frequencies for SFSB and TLB

The modal analysis is required to find the inherent dynamic properties of any fluid domain in terms of its natural frequencies. In CFD analysis, an impulse boundary load is applied to the tank wall surfaces, and free oscillation data is captured from the fluid domain. Then, the natural frequencies are computed from Fast Fourier Transformation (FFT) of free oscillation data. Fig. 7(a) and (b) show the first mode frequency computed from free vibration data generated through CFD analysis. Table 1 shows the first four natural frequencies for SFSB and TLB evaluated using CFD. And the natural frequencies are also determined through analytical formulae (Eq. (17)). The natural frequencies are found to be very close between CFD and analytical formulae.

3.3 Computation of slosh behavior using international seismic design codes

When excitation frequency is equal to the first mode natural frequency under zero damping condition, the liquid sloshing amplitude grows monotonically with time. For horizontal excitations, when excitation frequency is close to fundamental slosh frequency the free surface

Table 2 Slosh height using TID-7024 and ACI formulae for SFSB

Description		Length direction	Width direction	unit
Length of pool 2L		48.445	10.8	m
Width of pool W		10.8	48.445	m
Height of pool		9.5	9.5	m
Height of water (h)		8.7	8.7	m
Density of water		1000	1000	kg/m³
Mass of Water		455.2×10^4	455.2×10^4	kg
Acceleration (S_n)		0.0017	0.0263	g
		0.0167	0.2582	m/sec²
Displacement (A_1)		0.0508	0.0911	m
Convective frequency	ω	0.5732	1.684	rad/sec
	f	0.0912	0.2681	Hz
Impulsive Mass (m_i)		9.44×10^5	3.35×10^6	kg
Convective Mass (m_c)		34.4×10^5	1.47×10^6	kg
Convective shear force (V_c) at bottom of the wall		57	380	KN
Convective bending Moment at bottom of the wall (M_c)		0.25	2.1	MN-m
Convective over turning Moment at bottom of base slab. ($Mc*$)		1.8	3.13	MN-m
Slosh height TID-7024		0.0343	0.1234	m
Slosh height ACI 350.3 (2001)		0.0412	0.1421	m

undergoes resonance. (Kolukula and Chellapandi 2013, Eswaran *et al*. 2009). Table 2 shows the slosh height calculated using TID-7024 and ACI. The TID 7024 gives the slosh height during *x* direction excitation is 0.0343 m while that of ACI is 0.0412 m, similarly in *y* direction, slosh height is 0.123 m and 0.1421 m respectively from TID-7024 and ACI.

3.4 Computation of slosh height using CFD

Sloshing problems are usually attempted in CFD by applying the simulated random time-acceleration data as a volume force (Eswaran and Saha 2010). However, in this problem, an equivalent harmonic analysis is devised. The fraction of the steady state responds (u_j) that can be reached at *j*th cycle of excitations given by the following equation

$$\frac{|u_j|}{u_0} = 1 - e^{-2\pi d j} \tag{18}$$

as suggested by Chopra (2001), where *d* is the viscous damping (i.e., 0.005). The amplification for 0.005 damping under harmonic excitation is 100. The input amplitudes are taken corresponding figures from Figs. 3 and 4.

Modal calculation of slosh height of SFSB under first mode is described here. Here, *j* is taken as five. From Eq. (18), at 5th cycle, ratio of steady state to input acceleration is 0.1453(= $1-e^{-2\pi*0.005*5}$). Hence, amplification considering steady state response at 5th cycle is

0.1453×100×input acceleration. The *x* and *y* directions First mode frequencies are 0.0907 Hz and 0.267 Hz respectively (Table 1 and 2). And the response acceleration corresponds to these frequencies are 0.0167 m/s^2 and 0.258 m/s^2 respectively (From Fig. 3 and 4). Equivalent acceleration in *x* and *y* directions are 0.00115 m/s^2(=0.01667/(0.1453×100)) and 0.0178 m/s^2(=0.258/(0.1453×100)) respectively.

From above acceleration, amplitude can be computed as follows. The equivalent amplitude in *x* and *y* directions are 0.00349 m(=0.00114776/(0.5732×0.5732)) and 0.0063 m(=0.0178/(1.68×1.68)). Now, CFD analysis is performed for the first mode frequency with equivalent amplitude. So that, for first mode, slosh height in *x* direction is 0.03141 m(=9×0.00349) and in *y* direction is 0.1006 m(=16×0.00629). These calculations are shown in Table 3 in detail.

3.4.1 Horizontally excited SFSB in first mode

Figs. 8 and 10 show the first mode non-dimensional slosh height (ζ/A), where ζ is the mean level elevation and *A* is the maximum amplitude of excitation. Since here, harmonic excitation is applied as excitation, the equivalent amplitude for the harmonic excitation need to be evaluated. Due to the less damping, the time required to reach steady state response will be large. In view of this, the first five cycles are considered for analysis.
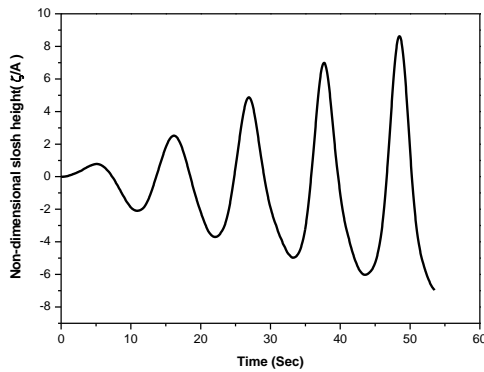
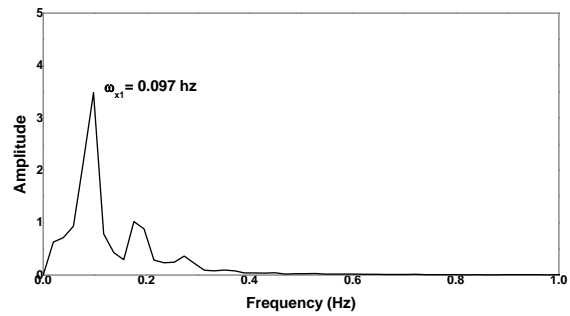Fig. 8 Non-dimensional slosh height at ω_{x1} for SFSB

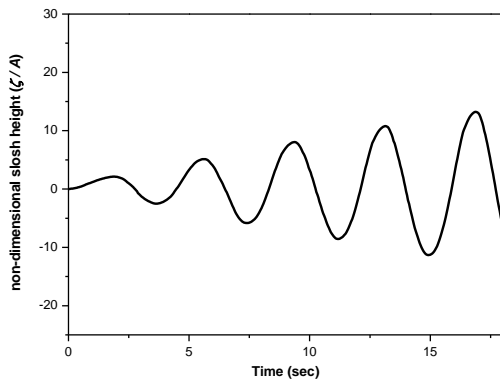Fig. 9 FFT of slosh height at ω_{x1} for SFSB

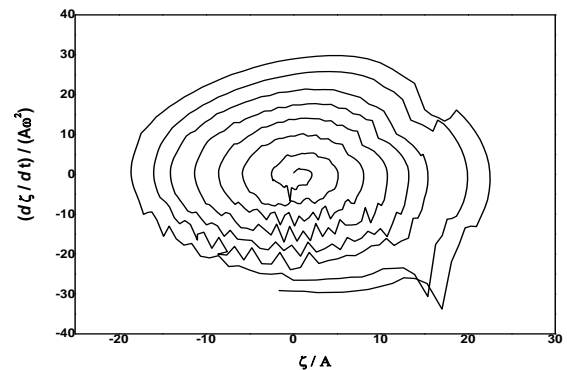Fig. 10 Non-dimensional slosh height at ω_{y1} for SFSB

Fig. 11 Phase plane diagram of slosh height at ω_{y1} for SFSB
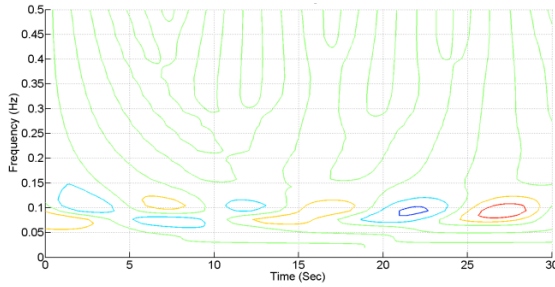
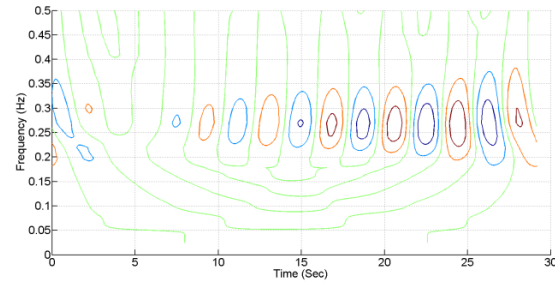Fig. 12 Wavelet coefficient for slosh height at ω_{x1} for SFSB

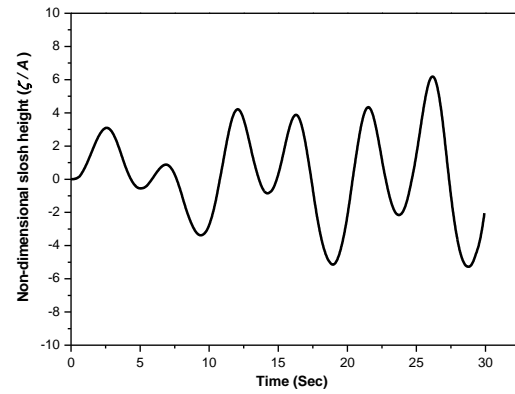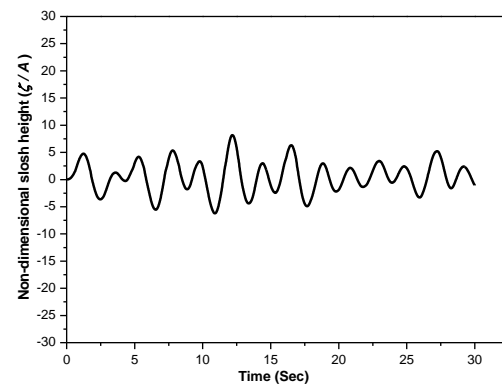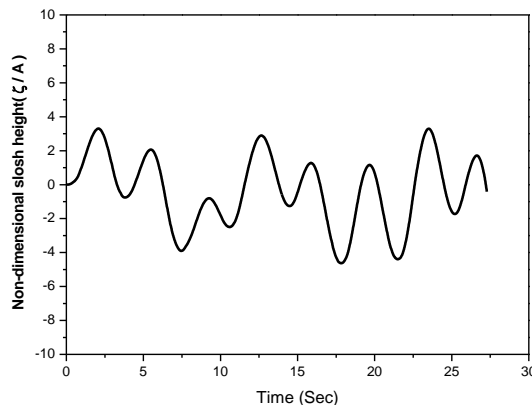Fig. 13 Wavelet coefficient for slosh height at ω_{y1} for SFSB
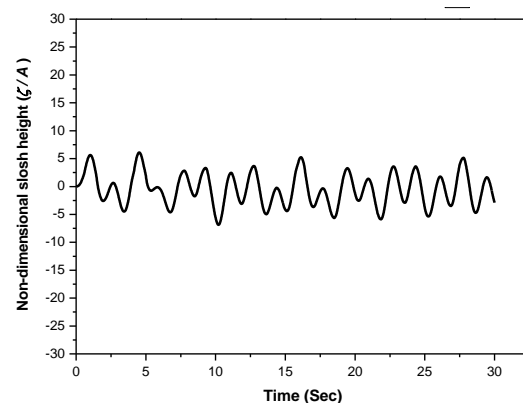

(a) *X* direction

(b) *Y* direction

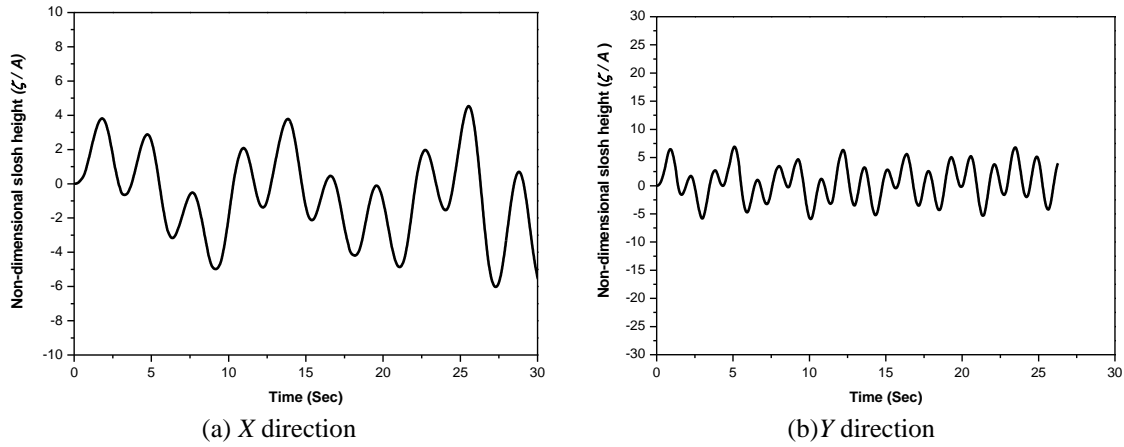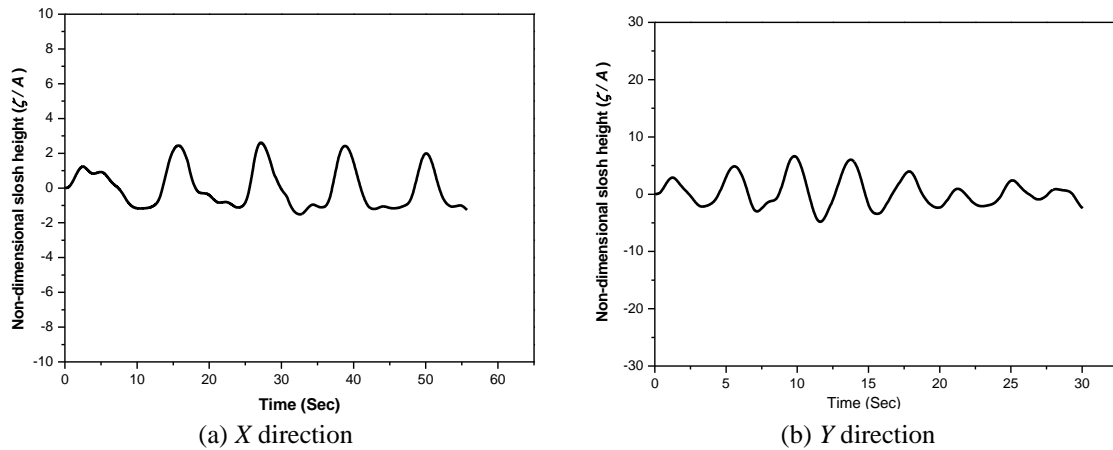Fig. 14 Non-dimensional slosh height for SFSB at second mode for *FR* 0.99

(a) *X* direction

(b) *Y* direction

Fig. 15 Non-dimensional slosh height for SFSB at third mode for *FR* 0.99

The frequency ratio (*FR*) (i.e., the ratio of excited frequency to corresponding natural frequency) is fixed as 0.99 for all the simulations. For the first mode frequency, the maximum ζ/A ratio is around 9 in longitudinal (*X*) direction excitation and 16 in lateral (*Y*) direction excitation at the end of 5th cycle (Figs. 8 and 10). FFT of SFSB slosh height under first mode *x* direction (ω_{x1})

(a) *X* direction   (b)*Y* direction

Fig. 16 Non-dimensional slosh height for SFSB at fourth mode for *FR* 0.99

(a) *X* direction   (b) *Y* direction

Fig. 17 Non-dimensional slosh height for SFSB due to combined modes for *FR* 0.99

excitation frequency is shown in Fig. 8. Since the excitation direction is first mode, the FFT of the slosh height data is shown the dominant frequency as 0.097 Hz. Phase plane diagram for slosh height at ω_{y1} for SFSB in Fig. 11. Phase plane diagram shows the nonlinearity existence in signal. Since *x* and *y* slosh height wave amplitudes are growing linearly, the phase plane diagram is showing in a circular path. The slosh height signals are analysed to get the frequency information along time using wavelet analysis. Figs. 12 and 13 show the wavelet analysis in *x* and *y* direction excitation at first mode. Real coefficients contour from the wavelet analysis shows the frequency details over time. Single dominant frequency is found in both cases (i.e., *x* and *y* direction) and not much varying with respect to time.

3.4.2 Horizontally excited SFSB in higher modes

Figs. 14 through 16 show the non-dimensional slosh height for frequency ratio (FR) 0.99 for first four modes. Fig. 17 shows the slosh height for the combined modes with FR 0.99. Slosh height obtained through CFD under first mode is 0.0318 m while from TID and ACI is 0.034 m

and 0.0411 m respectively. The CFD values are closely matching with the codal results. Seismic design codes do not have guidelines for the effect of higher modes and combined excitations. Hence, CFD investigation is performed for combined excitation along with higher modes. Initially, the combined effect in longitudinal and lateral directions are studied separately, (first four modes in *x* and *y* direction) and It is found that the slosh height is increased by 24.3% and 38.9% in *x* and *y* direction respectively.

3.4.3 Vertically excited SFSB

In most of the current seismic design codes, the responses due to vertical acceleration are usually taken into consideration by using about two thirds of the horizontal response spectra. However, from the recent studies one can conclude that the vertical to horizontal response spectral ratio depends on the distance of the site to the seismic source. This ratio is higher in the near-field region and in the high frequency range of the response spectra (Kianoush and Chen 2006). To investigate the effect due to vertical excitation, the excitation load is applied only in vertical direction along with gravity load (Eswaran *et al*. 2012). Fig. 18 shows the slosh height for vertically excited pool. During the vertical excitation, the standing waves are generated under the FRS design acceleration.
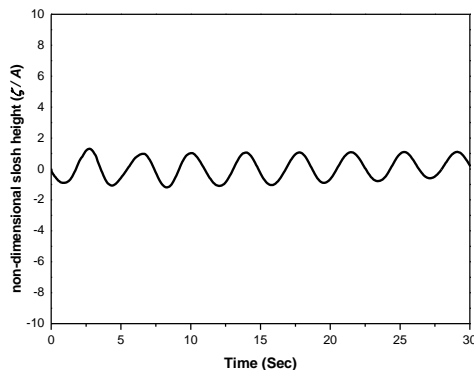

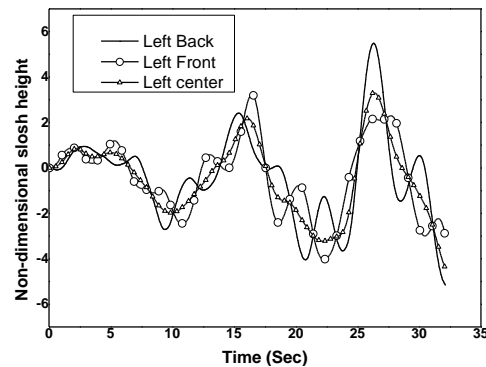Fig. 18 Vertically excited pool of SFSB

Fig. 19 Non-dimensional slosh height for horizontally & vertically excited SFSB in three directions
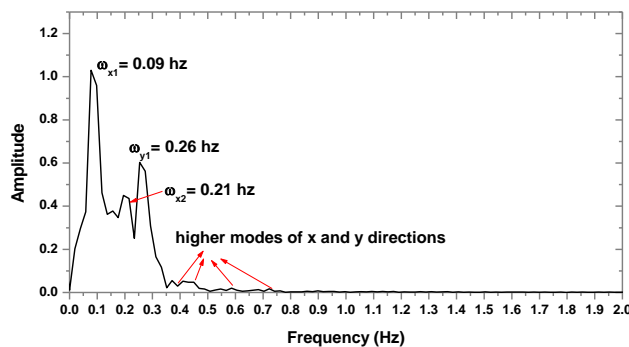

Fig. 20 FFT analysis of slosh height for horizontally & vertically excited SFSB in three directions
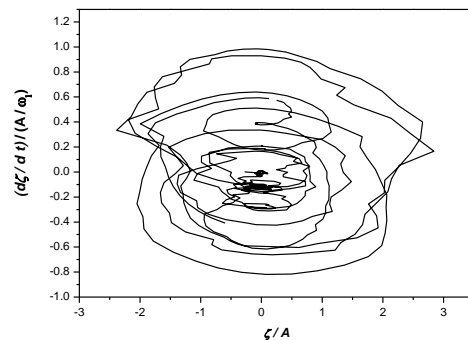

Fig. 21 phase-plane diagram of horizontally and vertically excited SFSB in three directions

3.4.4 Horizontally and vertically excited SFSB

Finally, to investigate the coupled effects of first four modes are applied in three directions (i.e., *x*, *y* and *z* directions) as excitation. Fig. 19 shows the difference of slosh height near tank left corner and center during combined excitation response of the horizontal and vertical acceleration. CFD analysis is also continued for combined excitation (longitudinal, lateral and vertical directions) along with higher modes, and found that the slosh height is increased to 0.235 m. And free board available is around 0.8 m. Hence there is no spillage as per given spectrum for SSE level of earthquake. To identify the dominant frequency, complete frequency analysis have been performed. Fig. 20 shows the FFT analysis of combined excitation slosh height at left back location while Fig. 21 shows the phase-plane diagram of horizontally and vertically excited SFSB in three directions. FFT analysis shows that first and second mode frequencies in *x* direction and first mode frequency *y* directions are dominant than other higher modes. However, the time versus frequency data is obtained from wavelet analysis to understand the frequency variation along the time. Three dominant frequencies can be identified from the wavelet analysis along the time (depicted in Fig. 22). This is illustrated by the contour plot of the real part of the wavelet coefficients shown in Fig. 22 where the scalograms are scattered by sloshing frequencies. The higher one scattered around frequency of 0.29 Hz while lower frequencies are scattered around 0.097 Hz and 0.213 Hz. Phase plane diagram show that the nonlinearity of the combined excitation.

All the slosh heights computed through CFD for SFSB at convective level and at free surface level acceleration are tabulated in Table 3 and Table 4 respectively. Initially, the slosh height values are shown for the first four mode frequencies separately. Thereafter, all the modes have been combined in lateral and longitudinal directions independently to find the effect of higher modes over the single mode. Now the slosh values are increased 24 % and 34 % in longitudinal and lateral direction respectively. Further, to study the influence of the multi-directional excitation, the CFD analysis is continued for combined excitation (longitudinal, lateral and vertical directions) along with higher modes, and found that the slosh height is increased drastically by 80%.

Slosh height values between CFD and TID 7024 and ACI are very close and deviation is negligible for the first mode. TID gave a simplified slosh height equation for higher modes (Eq.
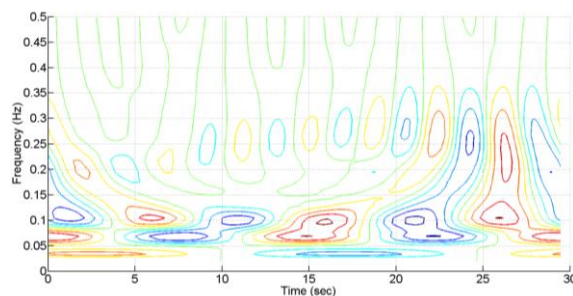

Fig. 22 Wavelet coefficient for slosh height signal of horizontally & vertically excited SFSB in three directions
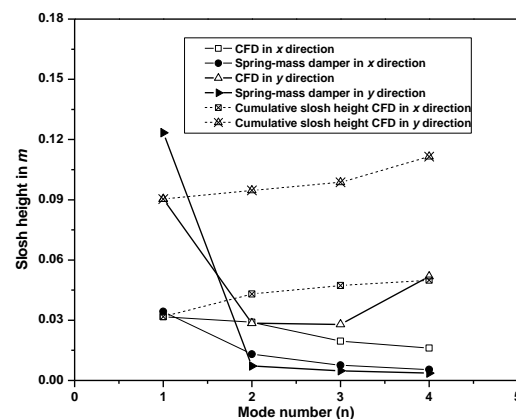

Fig. 23 CFD and TID (Spring and mass damper comparison for higher modes

(13)) for the rectangular tank and ACI is not giving any guidelines for the higher modes. Slosh height under higher modes is calculated through CFD and TID 7024 and shown in Fig. 23. Higher mode values are less than the CFD results in both x and y directions. Since TID uses a simplified straight forward equation for higher modes, it under predicts the slosh height over the CFD results.
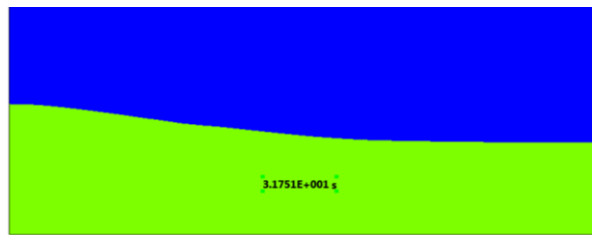
(a)
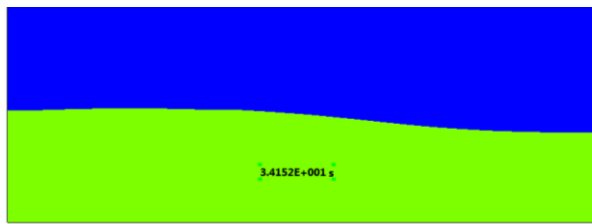
(b)
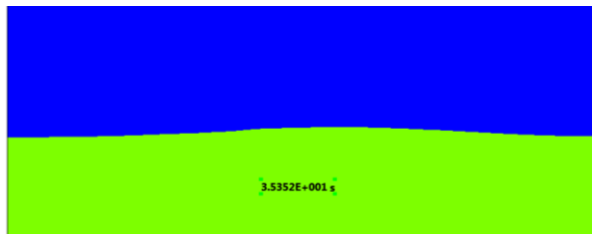
(c)

(d)

Fig. 24 Snapshot of sloshing in SFSB along *x* direction

(a)

(b)

(c)

(d)

Fig. 25 Snapshot of sloshing in SFSB along *y* direction
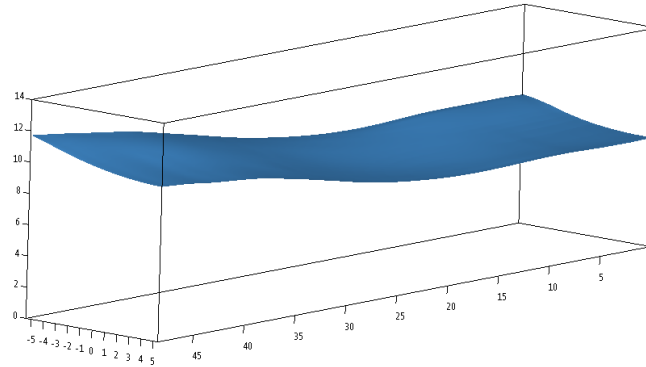
Fig. 26 Liquid free surface in 3D view during sloshing
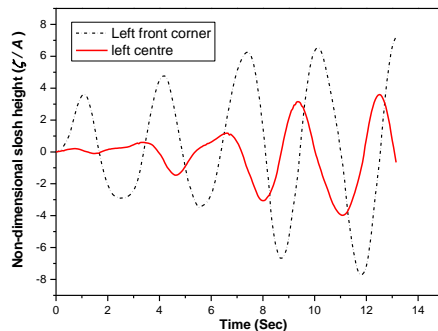
Fig. 27 Horizontally & vertically excited of TLB pool
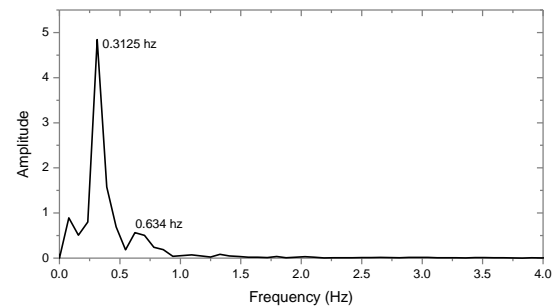
Fig. 28 FFT diagram of horizontally & vertically excited of TLB pool

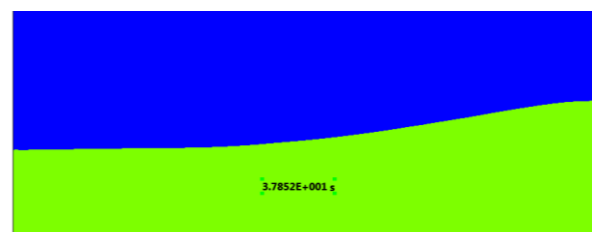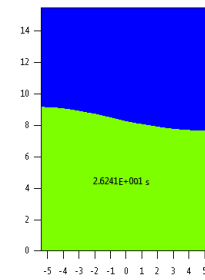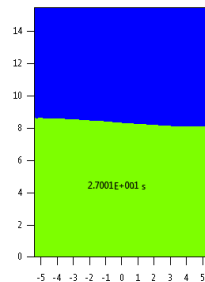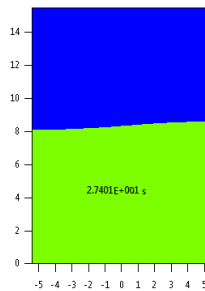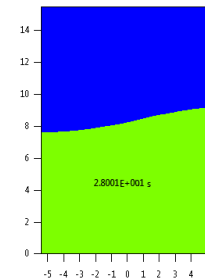In case of rectangular tank, the maximum slosh height is found in all the cases for SSE level of earthquake is 0.0318 m and 0.0903 m in longitudinal (x) and lateral (y) directions of pool respectively and slosh height for combined excitation with higher modes in three directions is 0.1535 m. TID provides a slosh height formula only for regular geometries (i.e., rectangular and cylindrical geometries). So it cannot be used for the complex geometries such as sectored tank. However, CFD can be used for any geometries to estimate the slosh height. As we found the fair comparisons between CFD and TID data, CFD can be used further for any complex geometries.

The pool corner has the slosh peak around 30 % to 40 % more than the single direction excitations slosh peak. Numerically, liquid acceleration at this corner is superimposing one over another. Since the FRS acceleration is very low, there is no much difference in slosh height. During the sloshing the liquid will get oscillate due to the external loading. A complete half cycle is shown. Figs. 24 and 25 show the snap shots SFSB x and y directions are shown in different time steps respectively. Three dimensional variation of free surface is depicted in Fig. 26.

3.5 Slosh height analysis for TLB

Similarly, Slosh height is investigated for TLB. TLB pool Slosh frequencies are listed in Table 5. Since the comprehensive study on effect of higher modes and combined excitations are

Table 3 Slosh height at convective level acceleration through numerical investigation

Mode	Direction	Frequency	Acceleration at convective level		Equivalent acceleration from harmonic excitation	Equivalent Amplitude from harmonic excitation	Non-dimensional slosh height	Slosh height of CFD at left corner	Slosh height of Spring-mass	Comments
		rad/sec	g	m/s2	m/s2	m		m	m	
					Horizontally excited SFSB					
1	x	0.57	0.0017	0.0167	0.0011	0.0035	9	0.0318	0.0343	First mode slosh height TID : 0.03433 m ACI: 0.041178 m
	y	1.68	0.0236	0.2315	0.0159	0.0056	16	0.0903	0.1234	TID : 0.12341 ACI: 0.142128
2	x	1.34	0.011	0.1079	0.0074	0.0041	7	0.0290	0.0131	Second mode
	y	2.92	0.045	0.4415	0.0304	0.0036	8	0.0285	0.0072	
3	x	1.78	0.023	0.2256	0.0155	0.0049	4	0.0196	0.0076	Third mode
	y	3.77	0.098	0.9614	0.0662	0.0047	6	0.0279	0.0048	
4	x	2.11	0.028	0.2747	0.0189	0.0042	3.8	0.0161	0.0054	Fourth Mode
	y	4.46	0.25	2.4525	0.1688	0.0085	6.1	0.0518	0.0036	
Combined 1-4	x	all	0.0637	0.6249	0.0430	0.0168	2.5	0.0420	0.0379	Combined effect of first four modes
	y	all	0.4166	4.0868	0.2813	0.0223	6.62	0.1480	0.1238	
					Vertically excited SFSB					
Combined 1-4	z	all	0.0637	0.6249	0.0430	0.0168	1.53	0.0257	0.0343	Combined effect of first four modes in vertical direction
					Horizontally and vertically excited SFSB					
Combined	xyz	all	0.4214	4.1343	0.28454	0.0280	8.39	0.135	0.0131	Combined effect of first four modes and three directional excitation
					Horizontally and vertically excited TLB					
Combined	xyz	all	0.5604	5.4972	0.3783	0.0301	7.29	0.219	0.0076	Combined effect of first four modes and three directional excitation

Table 4 Slosh height at free surface level acceleration through numerical investigation

Mode	Direction	Frequency	Acceleration at free surface level		Equivalent acceleration from harmonic excitation	Equivalent Amplitude from harmonic excitation	Non-dimensional slosh height	Slosh height at left corner	Comments
		rad/sec	g	m/s^2	m/s^2	M		m	
					Horizontally excited SFSB				
1	x	0.57	0.0009	0.0088	0.0006	0.0019	9	0.0168	First mode
	y	1.68	0.0201	0.1974	0.0136	0.0048	16	0.0770	
2	x	1.34	0.0122	0.1197	0.0082	0.0046	7	0.0321	Second mode
	y	2.92	0.0488	0.4784	0.0329	0.0038	8	0.0309	
3	x	1.78	0.0232	0.2280	0.0157	0.0050	4	0.0198	Third mode
	y	3.77	0.111	1.0890	0.0749	0.0053	6	0.0316	
4	x	2.11	0.0315	0.3092	0.0213	0.0048	3.8	0.0182	Fourth mode
	y	4.46	0.2496	2.4483	0.1685	0.00847	6.1	0.0517	
Combined 1-4	x	all	0.0679	0.6658	0.0458	0.0162	2.5	0.0405	Combined effect of first four modes
	y	all	0.4295	4.2131	0.2899	0.0224	6.62	0.1484	Combined effect of first four modes
					Vertically excited SFSB				
Combined 1-4	z	all	0.0637	0.6248	0.0430	0.0168	1.53	0.0248	Combined effect of first four modes in vertical direction
					Horizontally and vertically excited SFSB				
Combined	xyz	all	0.434	4.265	0.2936	0.0277	8.39	0.232	Combined effect of first four modes and three directional excitation

Table 5 Slosh height using TID-7024 and ACI 350.3 (2001) formulae for TLB

Description		Length direction	Width direction	unit
Length of pool 2L		6.972	6.5	m
Width of pool W		6.5	6.972	m
Height of pool		6.5	6.5	m
Height of water		5.7	5.7	m
Density of water		1000	1000	kg/m^3
Mass of Water		25.8 E+4	25.8 E+4	kg
Acceleration		0.031	0.346	g
		0.3041	0.3041	m/sec^2
Displacement (A_1)		0.0692	0.0911	m
Convective frequency	ω	2.0966	2.175	rad/sec
	f	*0.3337*	0.3464	Hz
Slosh height from TID-7024		0.0946	0.0882	m
Slosh height from ACI 350.3 (2001)		0.1081	0.1008	m

reported in above section for SFSB, whereas, for TLB, the slosh height for combined excitation is only evaluated and shown in Fig. 27 and corresponding FFT is shown in Fig. 28. The slosh height for combined excitation is 0.219 m. Slosh height in TLB from TID and ACI along length direction are 0.09456 m, 0.1081 m while along width direction are 0.08818 m and 0.1008 m. TLB the free board available is 0.8 m. And the maximum slosh height under SSE level of earthquake from the given spectrum along longitudinal (x) and lateral (y) directions of pool are around 0.1 m and 0.1 m respectively and the combined excitation with higher mode is found 0.219 m through CFD investigation. Hence there is no liquid spillage as per given SSE level of earthquake data at TLB.

4. Conclusions

During 1983 Nihonkai-chubu earthquake, the sloshing heights recorded are larger than that of computed linear conditions (Shimada *et al.* 1988). Usually, combined excitations with higher modes are 10-40% larger than those calculated under linear conditions. Similarly, in this work, the effects of higher modes and combined excitations on liquid sloshing are investigated through CFD simulations. From the above study, the following conclusions can be made.

(i) Along the length direction of SFSB, slosh height is obtained through CFD under first mode is 0.0318 m while from TID and ACI are 0.034 m and 0.0411 m respectively. Similarly, the width direction of SFSB slosh height values from CFD, TID and ACI are 0.0903 m, 0.123 m and 0.1421 m respectively. CFD values are closely matching with code results.

(ii) Seismic design codes do not have guidelines for the effect of higher modes and combined excitations. Hence, numerical investigation is extended to combined excitation along with higher modes. Initially, the combined effect in longitudinal and lateral directions are studied separately, (first four modes in x and y direction) and found that the slosh height is increased by 24.3% and 38.9% respectively.

(iii) CFD analysis is also continued for combined excitation (longitudinal, lateral and vertical

directions) along with higher modes, and found that the slosh height is increased drastically by 80%.

(iv) In case of SFSB, the maximum slosh height is found in all the cases for SSE level of earthquake is 0.042 m and 0.148 m in longitudinal (x) and lateral (y) directions of pool respectively and combined excitation with higher mode in three directions is 0.235 m. And free board available is around 0.8 m. Hence there is no liquid spillage as per given SSE level of earthquake data at SFSB.

(v) Slosh height in TLB from TID and ACI along length direction are 0.0946 m 0.1081 m while along width direction are 0.0882 m and 0.1008 m. TLB the free board available is 0.8 m. And the maximum slosh height under SSE level of earthquake from the given spectrum along longitudinal (x) and lateral (y) directions of pool are around 0.1 m and 0.1 m respectively and the combined excitation with higher mode is found 0.219 m through CFD investigation. Hence there is no liquid spillage as per given SSE level of earthquake data at TLB.

(vi) However, the corner of the pool has around 10-40 % higher slosh peak due to the combined effects. To avoid the over spilling at the corners of the pool, annular type angle horizontal baffles can be used.

(vii) To identify the dominant frequency, complete frequency analysis have been performed. FFT analysis shows that first and second mode frequencies in x direction and first mode frequency y directions are dominant than other higher modes. This is illustrated by the contour plot of the real part of the wavelet coefficients where the scalograms are scattered by sloshing frequencies. The higher one scattered around frequency of 0.29 Hz while lower frequencies are scattered around 0.097 Hz and 0.213 Hz.

(viii) Present CFD procedure can be opted for any irregular geometries to study effect of higher modes and combined three directional excitations since the codal provisions are not available.

Acknowledgements

References

ACI 350.3 (2001), "Seismic design of liquid containing concrete structures", *Am. Concrete Inst.*, Farmington Hill, MI, USA.

Alam, M.M. and Sakamoto, H. (2005), "Investigation of Strouhal frequencies of two staggered bluff bodies and detection of multi stable flow by wavelet analysis", *J. Fluid. Struct.*, **20**(3), 425-44.

Bedaoui, S., Afra, H. and Argoul, P. (2014), "Direct identification of modal parameters using the continuous wavelet transform, case of forced vibration", *Earthq. Struct.*, **6**(4), 393-408.

Benra, F.K., Dohmen, H.J., Pei, J., Schuster, S., and Wan, B. (2011), "A comparison of one-way and two-way coupling methods for numerical analysis of fluid-structure interactions", *J. Appl. Math.*, **2011**, Article ID 853560, 16.

Biswal, K.C., Bhattacharyya, S.K. and Sinha, P.K. (2006), "Non-linear sloshing in partially liquid filled containers with baffles", *Int J. Numer. Meth. Eng.*, **68**(3), 317-337.

Chang, Y.W., Gvildys, J., Ma, D.C., Singer, R., Rodwell, E. and Sakurai, A. (1989), "Numerical simulation

of seismic sloshing of LMR reactors", *Nuclear Eng. Des.*, **113**(3), 435-454.

Chen, B.F. and Nokes, R. (2005), "Time-independent finite difference analysis of 2D and nonlinear viscous liquid sloshing in a rectangular tank", *J. Comput. Phys.*, **209**, 47-81.

Chen, S., Johnson, D.B., Raad P.E. and Fadda, D. (1997), "The surface marker and micro cell method", *Int J. Numer. Meth. Fluid.*, **25**(7), 749-778.

Chopra A.K. (2001), *Dynamics of structures -Therory and applications to earthquake engineering*, Third reprint, Prentice-Hall of India Private Limited, NewDelhi.

Eswaran, M. and Saha U.K. (2011), "Sloshing of liquids in partially filled tanks-A review of experimental investigations", *Int. J. Ocean Syst. Eng.*, **1**(2), 131-155.

Eswaran, M., Goyal, P., Reddy, G.R., Singh, R.K. and Vaze, K.K. (2013), "Fluid-structure interaction analysis of sloshing in an annular - sectored water pool subject to surge motion", *Int. J. Ocean Syst. Eng.*, **3**(3), 1-21.

Eswaran, M., Virk, A.S. and Saha, U.K. (2013), "Numerical simulation of 3-D sloshing waves in a regularly and randomly excited container in vertical direction", *J. Marine Sci. Appl.*, **12**(3), 298-314.

Eswaran, M. and Saha, U.K. (2009), "Low steeping waves simulation in a vertical excited container using sigma transformation", *Proceedings of the 28th International Conference on Ocean, Offshore and Arctic Engineering*, Hawaii, USA.

Eswaran, M. and Saha, U.K. (2010), "Wave simulation in an excited cylindrical tank using sigma transformation", *Proceedings of the International Mechanical Engineering Congress & Exposition*, Vancouver, BC, Canada.

Eswaran, M., Saha, U.K. and Maity, D. (2009), "Effect of baffles on a partially filled cubic tank: Numerical simulation and experimental validation", *Comput. Struct.*, **87**(3-4), 198-205.

Eswaran, M., Singh, A. and Saha, U.K. (2010), "Experimental measurement of the surface velocity field in an externally induced sloshing tank", *J. Eng. Maritime Environ.*, **225**(2), 133-148.

Faltinsen, O.M., Rognebakke, O.F., Lukovsky, I.A. and Timokha, A.N. (2000), "Multidimensional modal analysis of nonlinear sloshing in a rectangular tank with finite water depth", *J. Fluid Mech.*, **407**, 201-234.

Frandsen, J.B. (2004), "Sloshing motions in excited tanks", *J. Comput. Phys.*, **196**, 53-87.

Fugal, D.L. (2009), *Conceptual wavelets in digital signal processing-an in-depth, practical approach for the non-mathematician*, Space & Signal Technologies LLC.

Housner, G.W. (1963), "Dynamic analysis of fluids in containers subjected to acceleration", *Nuclear Reactors and Earthquakes*, Report No. TID 7024, Washington D.C.,USA.

Kianoush, M.R. and Chen, J.Z. (2006), "Effect of vertical acceleration on response of concrete rectangular liquid storage tanks", *J. Eng. Struct.*, **28**, 704-715.

Kolukula, S.S. and Chellapandi, P. (2013), "Nonlinear finite element analysis of sloshing", *Adv. Numer. Anal.*, Article ID 571528.

Malhotra, P.K. (2004), *Seismic analysis of FM approved suction tanks*, Draft copy, FM Global, USA

Shimada, S., Noda, S. and Yoshida, T. (1988), "Nonlinear sloshing analysis of liquid storage tanks subjected to relatively long-period motions", *Proceedings of ninth world conference on earthquake engineering*, August, Japan.

Towhata, I. (2008), "History of geotechnical earthquake engineering in Japan", *The 14th World Conference on Earthquake Engineering*, October, Beijing, China.

Vosoughifar, H.R. and Naderi, M.A. (2014), "Numerical analysis of the base-isolated rectangular storage tanks under Bi-directional seismic excitation", *British J. Math. Comput. Sci.*, **4**(21), 3054-3067.

Xu, G., Hamouda, A.M.S. and Khoo, B.C. (2011), "Numerical simulation of fully nonlinear sloshing waves in three-dimensional tank under random excitation", *J. Ocean Syst. Eng.*, **1**(4), 355-372.

Yousefi, A.K., Nahvi, H. and Panahi, M.S. (2014), "Simulation, analysis and optimal design of fuel tank of a locomotive", *Struct. Eng. Mech.*, **50**(2), 151-161.

IT